Please cite this article in press as: Ulens et al., The Prokaryote Ligand-Gated Ion Channel ELIC Captured in a Pore Blocker-Bound Conformation by the Alzheimer's Disease Drug Memantine, Structure (2014), http://dx.doi.org/10.1016/j.str.2014.07.013

CellPress

The Prokaryote Ligand-Gated Ion Channel ELIC Captured in a Pore Blocker-Bound Conformation by the Alzheimer's Disease Drug Memantine

Chris Ulens,[1,*] Radovan Spurny,[1] Andrew J. Thompson,[2] Mona Alqazzaz,[2] Sarah Debaveye,[1] Lu Han,[3] Kerry Price,[2] Jose M. Villalgordo,[4] Gary Tresadern,[5] Joseph W. Lynch,[3] and Sarah C.R. Lummis[2]
[1]Laboratory of Structural Neurobiology, KU Leuven, Leuven 3000, Belgium
[2]Department of Biochemistry, University of Cambridge, Cambridge CB2 1QW, UK
[3]Queensland Brain Institute, University of Queensland, Brisbane QLD 4072, Australia
[4]VillaPharma Research, Murcia 30320, Spain
[5]Molecular Sciences, Janssen R&D, Beerse 2340, Belgium
*Correspondence: chris.ulens@med.kuleuven.be
http://dx.doi.org/10.1016/j.str.2014.07.013

SUMMARY

Pentameric ligand-gated ion channels (pLGIC) catalyze the selective transfer of ions across the cell membrane in response to a specific neurotransmitter. A variety of chemically diverse molecules, including the Alzheimer's drug memantine, block ion conduction at vertebrate pLGICs by plugging the channel pore. We show that memantine has similar potency in ELIC, a prokaryotic pLGIC, when it contains an F16'S pore mutation. X-ray crystal structures, using both memantine and its derivative, Br-memantine, reveal that the ligand is localized at the extracellular entryway of the channel pore, and the pore is in a more closed conformation than wild-type ELIC in both the presence and absence of memantine. However, using voltage clamp fluorometry we observe fluorescence changes in opposite directions during channel activation and pore block, revealing an additional conformational transition not apparent from the crystal structures. These results have important implications for drugs such as memantine, which block channel pores.

INTRODUCTION

The family of pentameric ligand-gated ion channels (pLGICs) or Cys-loop receptors includes nicotinic acetylcholine (nACh), serotonin (5-HT_3), γ-aminobutyric acid ($GABA_{A/C}$), and glycine (Gly) receptors. These receptors play an important role in fast synaptic neurotransmission by converting binding of a specific neurotransmitter that is released from the presynaptic terminal into a flux of ions across the membrane of the postsynaptic neuron. pLGICs are integral membrane proteins composed of an extracellular ligand-binding domain, an ion-conducting transmembrane domain, and an intracellular domain; prokaryotic homologs lack the intracellular domain. Receptor activation occurs through allosteric coupling between ligand binding and channel opening, upon neurotransmitter binding the extracellular domain is thought to undergo a conformational change that opens the channel gate and allows the passage of ions. Important progress in understanding these conformational changes at the structural level has been made recently with the X-ray crystal structure determination of the full-length prokaryote homologs ELIC (Hilf and Dutzler, 2008) and GLIC (Bocquet et al., 2009; Hilf and Dutzler, 2009), which may represent possible closed pore and open pore conformations, respectively. In addition, a crystal structure was also recently determined for GluCl (Hibbs and Gouaux, 2011), an invertebrate glutamate-gated chloride channel, which has a truncated intracellular domain to facilitate crystallization and is thought to also represent an open pore conformation.

A variety of chemically diverse molecules act as pore blockers of pLGICs, examples of such molecules are divalent cations, quaternary ammonium derivatives, aminoadamantanes such as memantine and rimantadine, lidocaine and quinacrine analogs, tricyclic antidepressants, and the neuroleptic chlorpromazine. Many of these channel blockers exert their effects by plugging the channel pore and inhibiting the flow of ions. For several decades channel blockers such as these have been highly instrumental in determining channel pore dimensions, identifying channel-lining residues, and in single channel studies (for recent reviews, see Bouzat, 2012; Sine, 2012). In 1977, Adams first demonstrated that pore blockers can bind both in open and closed channel states, as described for procaine blockade of the nACh receptor at the neuromuscular endplate (Adams, 1977). Recent cocrystal structures of GLIC revealed important structural insight into the mechanism of open channel block by showing the channel in an open pore conformation and bound by quaternary ammonium derivatives, divalent cations, or a lidocaine analog (Hilf et al., 2010). These structures showed that these channel blockers bind to the intracellular pore entryway or midway down the pore-lining M2-helix, and, as expected, do not cause a significant conformational change in the open pore.

Despite these recent insights, several important questions remain unanswered. Previous electrophysiological studies (Buisson and Bertrand, 1998) identified two separate binding sites in the channel pore of α4β2 nACh receptors based on the fraction

STFODE 2983

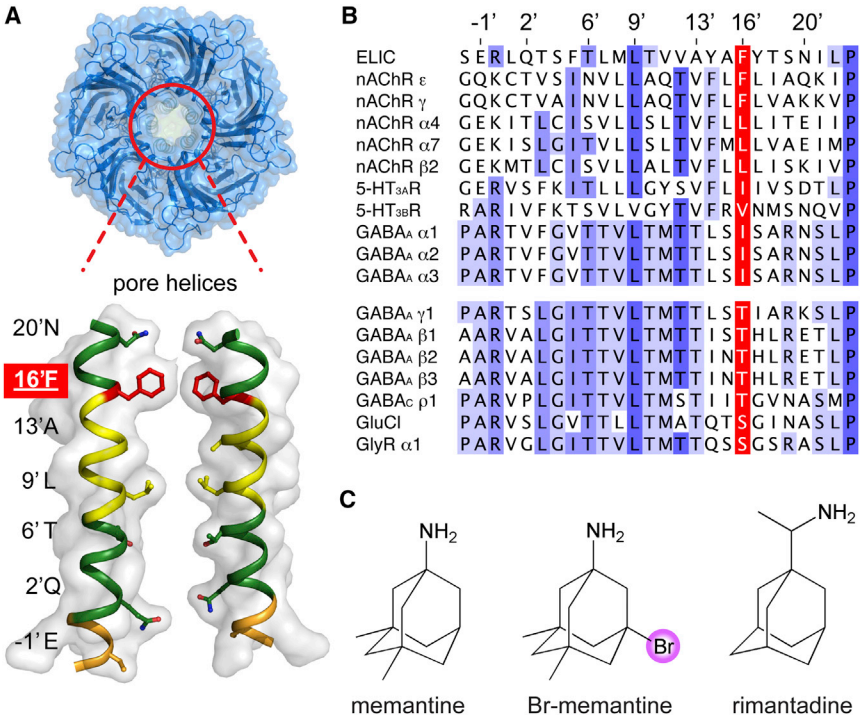

Figure 1. An Unusual Phenylalanine Residue Restricts Pore Access in ELIC

(A) Cartoon representation of ELIC with transparent surface overlaid in blue and seen along the 5-fold symmetry axis from the extracellular side of the channel. The inset shows a detailed sideways view of the pore-lining M2-helices of two opposing subunits. Hydrophilic parts of the ion conduction pathway are colored in green, hydrophobic in yellow, and charged in orange. The white transparent surface representation highlights the pore constriction point formed by the 16'F residues (red sticks).

(B) Sequence alignment of ELIC with human pLGICs. 16'F residues are found only in nAChR ε- and γ-subunits. 5-HT_3 receptors and $GABA_A$ α-subunits contain hydrophobic residues (Leu, Val, or Ile), whereas GABA receptor β-, γ-, and ρ-subunits, GluCl and Gly receptors contain hydrophilic residues (Thr or Ser). Residues are colored in shades of blue according to sequence conservation set at an identity threshold of 40%; 16' residues are colored in red.

(C) Structure formulas of the pore blockers used in this study.

of the transmembrane electrical field sensed by the pore blocker. There is one of these sites that is located near the middle of the field across the ion pore and may be equivalent to the lidocaine binding site identified in the open GLIC structure (Hilf et al., 2010). The second site is located closer to the extracellular entryway of the channel pore, as pore blockers at this site sense a significantly smaller fraction of the transmembrane electrical field (Buisson and Bertrand, 1998). Consequently, Buisson and Bertrand deduced that channel blockers which inhibit α4β2 nACh receptors can bind to distinct locations within the ion pore (Buisson and Bertrand, 1998). These data pose several questions: Where is the second pore blocker site at the extracellular entryway of the channel pore located? What are the structural determinants of blocker recognition at this binding site? What is the structural mechanism of blocker trapping in a closed channel conformation, and do conformational changes accompany this transition?

As recently demonstrated, ELIC forms cation-selective channels that are inhibited by divalent cations (Zimmermann et al., 2012), and a number of compounds that inhibit vertebrate pLGICs also inhibit ELIC (Thompson et al., 2012), making it a potentially suitable model for structural and functional studies of eukaryotic cation-selective pLGICs. In this study, we demonstrate that the ELIC pore mutant F16'S reliably replicates the blocker sensitivity observed in vertebrate pLGICs. Using X-ray crystallography, we reveal that memantine, which is therapeutically used in the treatment of Alzheimer's disease, binds in the upper half of the channel pore of the F16'S mutant. Voltage clamp fluorometry reveals that memantine induces distinct movements at the outer region of the pore, although the fact that we observed no obvious structural changes suggests this is an unstable or short-lived memantine-induced state.

RESULTS AND DISCUSSION

F16'S Increases the Sensitivity of ELIC to Channel Blockers

We previously demonstrated that ELIC is activated by GABA and modulated by benzodiazepines with effects similar to those observed at eukaryote $GABA_A$ receptors (Spurny et al., 2012). In addition, we previously found that a wide range of known pLGIC channel blockers also inhibit ELIC (Thompson et al., 2012). At the structural level, the ELIC pore is unusual in that it contains a bulky phenylalanine residue at the 16' position, located at the extracellular entrance of the channel pore (Figure 1A). Because of the pentameric symmetry of the protein, the 16'F residues form a narrow constriction that reduces the pore radius to less than 1.5 Å. In eukaryote nACh receptors, the 16'F residue is found only in the ε- and γ-subunits, with α- and β-subunits containing the smaller hydrophobic Leu residue (Figure 1B). Hydrophobic residues (Leu, Ile, or Val) are also found in 5-HT_{3A-E} receptors and $GABA_A$ receptor α-subunits at the same location. In contrast, hydrophilic residues (Thr or Ser) are found in $GABA_A$ receptor β- and γ-subunits, $GABA_C$ receptors, Gly receptors, and the glutamate-activated chloride channel GluCl. In GLIC, the channel pore contains an Ile residue at the homologous 16' position, which is likely to be a less stringent barrier than phenylalanine, and possibly explains why GLIC has an enhanced sensitivity for channel blockers when compared to ELIC (Hilf et al., 2010; Thompson et al., 2012).

To test this hypothesis, we generated a F16'S ELIC mutant and tested it in *Xenopus* oocytes and human embryonic kidney (HEK) cells. In oocytes, we observed a small increase in GABA half-maximal value of activation (EC_{50}) compared to wild-type ELIC (6.6 mM versus 1.6 mM, Table 1), as has been previously reported for a F16'A mutant (Zimmermann and Dutzler, 2011),

STFODE 2983

Please cite this article in press as: Ulens et al., The Prokaryote Ligand-Gated Ion Channel ELIC Captured in a Pore Blocker-Bound Conformation by the Alzheimer's Disease Drug Memantine, Structure (2014), http://dx.doi.org/10.1016/j.str.2014.07.013

Table 1. Concentration-Response Relationships for WT ELIC and F16'S in Ca^{2+}-free ND96

GABA	pEC_{50}	EC_{50} (mM)	nH	n
Wild-type	2.78 ± 0.04	1.6	2.5 ± 0.7	7
F16'S	2.18 ± 0.06	6.6	2.6 ± 0.6	3
Memantine	pIC_{50}	IC_{50} (μM)	nH	n
Wild-type	3.93 ± 0.02	118	1.7 ± 0.1	5
F16'S	5.08 ± 0.07	8.3	0.9 ± 0.1	4
Rimantadine	pIC_{50}	IC_{50} (μM)	nH	n
Wild-type	4.27 ± 0.03	54	1.0 ± 0.2	4
F16'S	5.73 ± 0.03	1.9	1.1 ± 0.1	3

indicating that the 16' position may influence channel gating. Then, we tested the effect of the F16'S mutation on pore blocker sensitivity using the aminoadamantane derivatives memantine and rimantadine as probes (Figure 1C). Rimantadine is an antiviral drug that we have previously identified as being one of the most potent pore-blocking compounds in ELIC (Thompson et al., 2012). In addition, rimantidine blocks the viral M2 channel (Schnell and Chou, 2008; Stouffer et al., 2008), and it also inhibits GLIC and other pLGICs (Alqazzaz et al., 2011). Memantine is structurally similar to rimantidine; it is clinically used in the treatment of Alzheimer's disease, likely improving cognition through channel block of N-methyl-D-aspartate receptors; it also blocks the pore of α7 nACh receptors with similar or higher potency, but whether therapeutic effects are mediated through these nACh receptors is currently debated (Aracava et al., 2005; Oliver et al., 2001; Rammes et al., 2001; Rogawski and Wenk, 2003). Testing these compounds on the F16'S mutant revealed that the sensitivity is enhanced ~30-fold for rimantadine and ~15-fold for memantine (Table 1). In HEK cells, the data reveal that both compounds show mixed inhibition (Figure S1 available online), as concentration-response curves show an increase in EC_{50} and a decrease in the maximum response (R_{max}), suggesting possible actions at both the agonist binding site and the channel pore.

These results point to an important role of 16'F in reducing the sensitivity of ELIC to pore blockers, possibly by restricting access to the channel pore. This restriction is relieved in ELIC F16'S, which displays a sensitivity to pore blockers that is more similar to eukaryote receptors.

X-Ray Crystal Structures of F16'S ELIC Blocked by Memantine

To advance our understanding of the molecular determinants of channel blockers at the structural level, we determined X-ray crystal structures of ELIC F16'S in complex with memantine or its brominated derivative Br-memantine (Figure 1C). Such a bromine substitution greatly facilitates structural studies as bromine generates an anomalous diffraction signal and aids in identifying the ligand-binding pose in electron density maps. The crystal structures of ELIC in complex with memantine or Br-memantine were determined from X-ray diffraction data at a resolution of 3.2 Å and 3.9 Å, respectively (crystallographic statistics are shown in Table 2). These data are of medium resolution, but in both structures, inspection of the Fourier F_o–F_c difference map reveals clear peaks at a contour level of 4σ at two different sites in ELIC, one localizing to the extracellular domain (Figures 2A–2C) at a site that overlaps with the agonist binding site and another in the channel pore (Figures 2D–2G). The binding of memantine at these two distinct sites is further substantiated by the anomalous difference map of the Br-memantine cocrystal structure, which clearly shows peaks (magenta mesh in Figures 2C and 2G is contoured at 4.5σ for the pore site and 6σ for the agonist binding site) at all five agonist-binding sites in the extracellular domain and one peak in the channel pore. Notably, we also observe F_o–F_c difference density near the 6' residue in the memantine cocrystal structure, but weaker F_o–F_c density and no anomalous density in the bromo-memantine structure. Therefore, we believe it could be a cation or water molecule stabilized near the 6' residue. The bromine atom in the Br-memantine molecule is attached at a position that is perpendicular to the amine-moiety (Figure 1C), which allows us to assign a likely binding pose for this relatively symmetric ligand. Specifically, in the agonist-binding site we observe that the anomalous peak is slightly offset toward the (−) subunit compared to the simple difference density peak (Figure 2C). This suggests a likely binding pose for Br-memantine (Figure 2B) in which the bromine atom points toward Y38 (loop D) and the amine-moiety is stabilized by cation-π interactions on the (+) subunit with residues F188 (loop C) and F133 (loop B), which is similar to the cation-π interactions observed for the ELIC agonist GABA (Spurny et al., 2012). Little to no conformational change is observed at the tip of loop C and loop F, which contrasts the movement of these loops induced by the competitive antagonist acetylcholine (Pan et al., 2012). The Br-memantine and memantine binding pose strongly overlaps with the GABA binding pose we recently reported (Spurny et al., 2012), suggesting that memantine can act as a competitive antagonist in the extracellular ligand-binding site. This result is consistent with earlier observations that the inhibition of eukaryote nACh receptors by relatively low concentrations of memantine is voltage-independent and binds at a site in the extracellular domain (Aracava et al., 2005). In contrast, inhibitory effects of relatively high concentrations of memantine become voltage-dependent, suggesting an interaction in the channel pore (Aracava et al., 2005).

In agreement with this observation, we find in the crystal structures that Br-memantine and memantine bind in the channel pore (Figures 2D and 2E) at a position that lies between the 13'A and 16'S residues that are located in the extracellular half of the pore-lining M2-helix (Figure 2F). Clearly, the interpretation of the electron density is more complicated at this site (Figure 2G) given the symmetry mismatch between the pentameric channel pore and the pyramidal-shaped memantine molecule. Nevertheless, we observe that the anomalous difference density is slightly offset toward the middle of the channel pore compared to the simple difference density (Figure 2G). This suggests a likely binding pose for Br-memantine in which the amine-moiety points toward the hydrophilic upper part of the pore (Figures 2E and 2F). We believe that the opposite orientation, in which the amine-moiety points toward the hydrophobic middle part of the pore (9'L and 13'A), is energetically less favorable.

Comparison of the ELIC F16'S memantine-bound structure with the published crystal structure for wild-type ELIC in the apo state (Hilf and Dutzler, 2008) (Protein Data Bank [PDB] code 2VL0) reveals important differences. As expected,

STFODE 2983

Table 2. Crystallographic Data Collection and Refinement Statistics

	ELIC F16'S + Memantine	ELIC F16'S + Br-Memantine (Data Set 1)	ELIC F16'S + Br-Memantine (Data Set 1 and 2)	ELIC F16'S apo
Crystallographic Statistics				
Beamline	X06A (SLS[a])	X06A (SLS[a])	X06A (SLS[a])	X06A (SLS[a])
Date of collection	September 25, 2012	November 10, 2012	November 10, 2012	March 30, 2014
Wavelength (Å)	0.9999	0.91946	0.91946	0.9999
Spacegroup	$P2_1$	$P2_1$	$P2_1$	$P2_1$
a,b,c (Å)	105.48, 265.28, 111.10	106.50, 266.09, 112.18	106.33, 266.05, 111.92	105.9, 264.97, 111.33
β (°)	110.28	107.70	107.78	108.82
Resolution limits (Å)	49.47 – 3.2 (3.37 – 3.2)	49.83 – 3.90 (4.11 – 3.90)	49.73 – 5.0 (5.27 – 5.0)	48.96 – 3.60 (3.79 – 3.60)
R_{merge} (%)	9.0 (89.8)	13.7 (93.6)	11.5 (29.2)	14.7 (99.3)
$<I/\sigma>$	12.5 (1.5)	8.7 (1.5)	18.6 (9.3)	8.4 (1.5)
Multiplicity	3.5 (3.3)	4.9 (4.9)	14.1 (13.3)	3.9 (4.0)
Completeness (%)	99.8 (99.7)	99.3 (95.5)	99.9 (100.0)	99.9 (100.0)
Total number of reflections	328,872 (45,224)	260,800 (36,496)	362,083 (49,830)	260,535 (39,343)
Number unique reflections	93,823 (13,615)	53,624 (7,432)	25,615 (3,740)	66,992 (9,751)
Anomalous completeness		97.5 (92.2)	99.8 (99.9)	
Anomalous multiplicity		2.5 (2.5)	7.1 (6.6)	
Refinement and Model Statistics				
R_{work} (%)	19.9	20.21		22.01
R_{free} (%)	25.22	24.99		26.34
Rmsd bond distance (Å)	0.013	0.009		0.009
Rmsd bond angle (°)	1.71	1.56		1.589
Ramachandran analysis				
Outliers (%)	2.95	1.61		2.30
Favored (%)	90.95	91.28		90.36
Average B factors (Å^2)				
Protein	120.414	142.443		118.71
Ligand	107.953	131.125		
MolProbity score (%)	83	95		91

[a]Swiss Light Source

substitution of the bulky 16'F residue by the smaller serine residue causes a considerable widening of the channel pore at this position (Figures 3A and 3B), thereby relieving the restricted pore access imposed by the phenylalanine side chains. Consequently, the pore radius increases from <2 Å at the 16'F position to ~4 Å following 16'S substitution (Figure 3C), a change that is sufficient to permit access of the blocker to the binding site just below the 16'S position. Remarkably, we also observe that the pore widening is partially compensated by a contraction of the M2-helices around the memantine molecule. This becomes apparent upon superposition of F16'S ELIC and wild-type apo ELIC (Figures 3D and 3E), which shows an inward movement of the M2-helices at their extracellular ends, and a 2° tilt over residue 6'T. An important question is whether this inward movement of the M2-helices is caused by the F16'S mutation, memantine binding, or a combination of both. To address this question, we determined the crystal structure of F16'S apo structure at a resolution of 3.5 Å. In the F16'S apo structure, we observe an inward movement of the M2-helices that is similar to F16'S ELIC with memantine bound. This result suggests that the observed movement in F16'S ELIC with memantine bound is caused in part by the mutation rather than ligand binding.

Conformational Pore Dynamics upon Channel Block by Memantine

To determine if memantine causes a conformational change that is not apparent from the structural data, we used voltage clamp fluorometry (VCF) on *Xenopus* oocytes expressing ELIC F16'S. This technique involves the incorporation of a cysteine residue into a domain of interest and labeling it with a sulfhydryl-reactive, environmentally sensitive fluorescent dye. Possible changes in fluorescence due to movement of the domain to a different local environment are then simultaneously recorded with channel currents. This approach permits a direct correlation between conformational changes of the labeled domain and channel gating, measured in real time. To this end, we engineered the F16'S mutation in the background of an otherwise cysteine-free channel, except for a cysteine residue incorporated at the 19' position, which is localized at the top of the M2-helix (Figure 4A). Fluorophores attached to the homologous 19'C mutation have been exploited in VCF studies on other pLGICs, where

STFODE 2983

Please cite this article in press as: Ulens et al., The Prokaryote Ligand-Gated Ion Channel ELIC Captured in a Pore Blocker-Bound Conformation by the Alzheimer's Disease Drug Memantine, Structure (2014), http://dx.doi.org/10.1016/j.str.2014.07.013

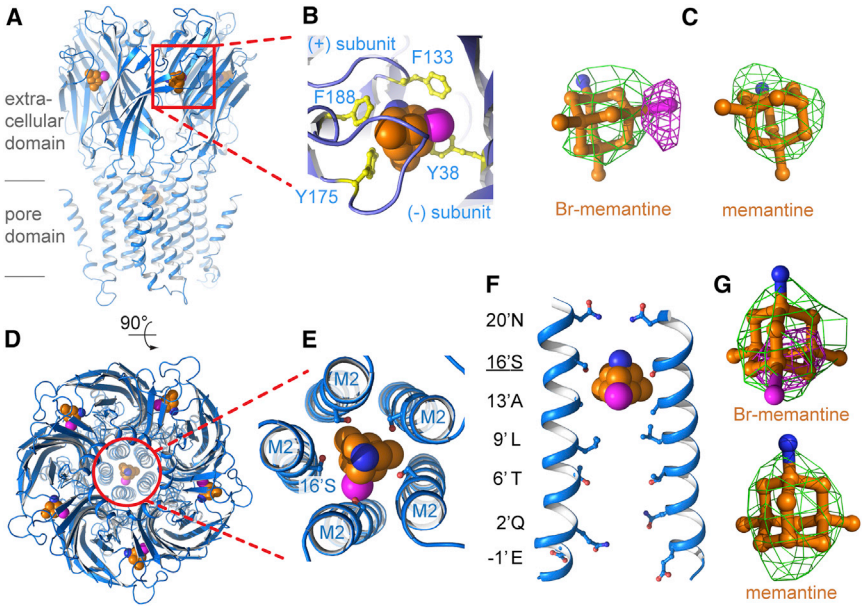

Figure 2. Crystal Structures of ELIC F16'S with Memantine Bound

(A) Sideways cartoon view of X-ray crystal structure of ELIC F16'S in complex with bromo-memantine. Br-memantine is shown in sphere representation (orange is carbon, blue is nitrogen, and magenta is bromine).

(B) Detailed view of molecular recognition of Br-memantine in the agonist-binding site formed at the extracellular interface between the (+) subunit and (−) subunit. Conserved aromatic residues of the agonist-binding site are highlighted in yellow stick representation.

(C) Experimental electron densities observed at this site for Br-memantine and memantine (molecules are shown in ball and stick representation). F_o–F_c difference density peaks are shown as a green mesh and at a contour level of 4σ. The anomalous difference density peak is shown as a magenta mesh and at a contour level of 6σ.

(D) Top cartoon view of ELIC F16'S in complex with Br-memantine. The inset in (E) shows a detailed view of a single Br-memantine molecule bound in the pore of the channel.

(F) Sideways view of pore-lining M2-helices from two opposing subunits. The Br-memantine molecule is bound at the extracellular entryway of the channel pore between the 13'A and 16'S residues.

(G) Experimental electron densities observed for Br-memantine and memantine in the pore site. F_o–F_c difference density peaks are shown as a green mesh (4σ) and anomalous difference density as a magenta mesh (4.5σ).

they act as reliable reporters of conformational changes of the M2 domain during channel gating (Pless et al., 2007; Wang et al., 2010).

VCF recordings were carried out in Ca^{2+}-containing ND96 and showed that unlabeled F16'S+S19'C ELIC has a sensitivity to GABA (EC_{50} = 39 mM, Table 3) and the full agonist propylamine (Zimmermann and Dutzler, 2011) (EC_{50} = 740 μM), that are comparable to wild-type (21 mM and 446 μM, respectively [Spurny et al., 2012; Zimmermann and Dutzler, 2011]). In addition, F16'S+S19'C has sensitivity to memantine that is comparable to F16'S ELIC (half-maximal value of inhibition [IC_{50}]= 54 μM, Table 3). After fluorescent labeling of F16'S+S19'C ELIC with methanethiosulfonate-rhodamine (MTSR), the agonist and blocker sensitivities also remain relatively similar (EC_{50} GABA = 50 mM, EC_{50} propylamine = 870 μM, IC_{50} memantine = 91 μM, Table 3). For VCF recordings, we applied 150 μM memantine (pore blocker) or 20 mM propylamine (full agonist). For memantine, we observe a negative deflection in the fluorescence (Figure 4B, ΔF_{max} = −1.56 ± 0.81%, n = 6), whereas the full agonist propylamine evokes a positive deflection in the fluorescence

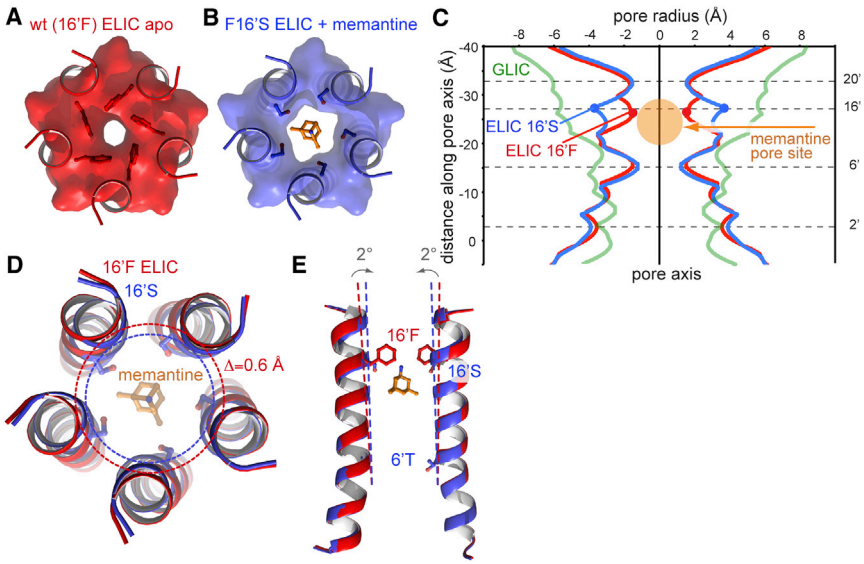

Figure 3. Pore Closure Traps a Memantine Molecule

(A and B) Surface representation of the extracellular entryway of the ELIC channel pore for WT ELIC apo (Hilf and Dutzler, 2008) (red transparent surface, A) and ELIC F16'S (blue transparent surface, B). 16' residues are shown as sticks. Memantine is shown in orange sticks.

(C) Pore radius calculated for WT ELIC apo (red), ELIC F16'S (blue), and GLIC (Bocquet et al., 2009; Hilf and Dutzler, 2009) (green). Red and blue dots highlight the difference in pore radius near 16' residues. The orange arrow indicates the approximate location of the memantine binding site in the channel pore.

(D) Cartoon representation of the α helical backbone for WT apo and F16'S ELIC. This cartoon illustrates that the pore widening near F16'S is partially compensated by a contraction of the pore domain around the memantine molecule. The distance movement of the M2-helix is 0.6 Å as measured between the Cα atoms of the 16' residues.

(E) Sideways view of the ELIC pore highlights a 2° tilt of the M2-helices around the 6'T residue.

STFODE 2983

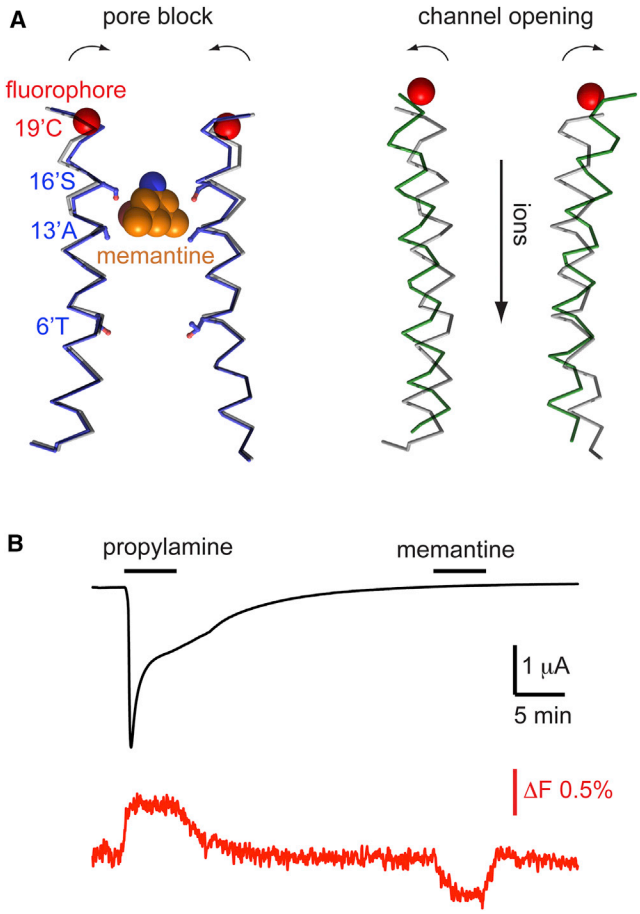

Figure 4. Voltage Clamp Fluorescence Shows Conformational Change of M2 by Memantine

(A) Ribbon representation of pore-lining M2-helices and memantine shown in sphere representation. The red sphere indicates the location of the fluorophore attached to 19'C.

(B) VCF recording of ELIC F16'S fluorescently labeled at S19'C using MTSR. Channels were activated with 20 mM of the agonist propylamine (Zimmermann and Dutzler, 2011) and blocked with 150 μM memantine. Fluorescence deflections are in opposite directions during channel opening compared to pore block.

(Figure 4B, ΔF_{max} = +2.16 ± 0.34%, n = 6). The fluorophore MTSR responds with an increase in quantum efficiency as the hydrophobicity of its local environment increases (Dahan et al., 2004). Consequently, it can be deduced that the 19' residue moves to a more hydrophobic environment during channel opening and a more hydrophilic environment during pore block by memantine. From the perspective of published ELIC and GLIC crystal structures, the agonist-induced local change could be interpreted in the context of an outward M2-tilt during channel opening (Bocquet et al., 2009; Hilf and Dutzler, 2009). The structural basis of the memantine-induced conformational change is unclear, although it must be different to that produced by the agonist. As the memantine-induced conformational change is not apparent in the crystal structure, we conclude that it represents either a subtle conformational change or an unstable or short-lived state that is not amenable to crystallization.

Table 3. Concentration-Response Relationships for F16'S+S19'C ELIC before and after Fluorescent Labeling Ca^{2+}-Containing ND96

GABA	pEC_{50}	EC_{50} (mM)	nH	n
F16'S + S19'C unlabeled	1.41 ± 0.07	39	1.5 ± 0.3	4
F16'S + S19'C labeled	1.30 ± 0.02	50	4.2 ± 1.6	4
Memantine	pIC_{50}	IC_{50} (μM)	nH	n
F16'S + S19'C unlabeled	4.27 ± 0.01	54	0.8 ± 0.1	5
F16'S + S19'C labeled	4.04 ± 0.16	91	1.0 ± 0.1	5

Conclusions

Understanding the structural determinants of pore block in open and closed conformations of a channel is fundamental in ion channel biology. In this study, we have revealed the crystal structure of a prokaryote model ion channel ELIC captured in a pore-blocker bound conformation. We find that the pore blocker memantine, which is clinically used as an Alzheimer's disease drug, binds at a site in the extracellular entryway of the pore (Figure 5), which likely corresponds to a previously identified peripheral site that senses only a small fraction of the transmembrane electrical field (Buisson and Bertrand, 1998). VCF demonstrated that memantine elicited a conformational change distinct from that of a channel opener at the extracellular region of the M2 domain, although no alterations in this region were apparent in the crystal structure. We infer that memantine induces a short-lived or unstable state, which differs from that induced by an agonist. This result is important in understanding the mechanisms of action of pore-binding drugs.

Our finding emphasizes the conformational flexibility of the channel pore and demonstrates a closed conformation to the currently known collection of conformational states of both ELIC and other pLGICs, which include an open state of an L9'- and F16'-mutated ELIC (Gonzalez-Gutierrez et al., 2012), GLIC at acidic pH (Bocquet et al., 2009; Hilf and Dutzler, 2009), and GluCl with ivermectin and glutamate (Hibbs and Gouaux, 2011), as well as different possible closed states, namely apo ELIC (Hilf and Dutzler, 2008), the locally closed state as observed in cysteine-crosslinked GLIC (Prevost et al., 2012) and the presumed resting or closed state of GLIC at neutral pH (Sauguet et al., 2014). The insights derived from our study on ELIC likely extend to the other members of the pLGIC family and have implications for the rational design of new pore blocker drugs with therapeutic importance.

EXPERIMENTAL PROCEDURES

Two-Electrode Voltage Clamp Recordings

For electrophysiological recordings from *Xenopus* oocytes, stage V–VI oocytes were injected with 10 ng ELIC mRNA and incubated at 18°C until the day of recording. ELIC cDNA was cloned into the pGEM-HE expression vector and mRNA was transcribed in vitro using the mMESSAGE mMACHINE T7 transcription kit (Ambion) as previously described (Spurny et al., 2012). Mutants were engineered using a QuikChange strategy (Stratagene) and verified by sequencing.

Using two-electrode voltage-clamp, *Xenopus* oocytes were clamped at −60 mV using an OC-725 amplifier (Warner Instruments), Digidata 1322A, and the Strathclyde Electrophysiology Software Package (Department of Physiology and Pharmacology, University of Strathclyde, UK). Currents were recorded at 5 kHz and filtered at a frequency of 1 kHz. Micro-electrodes

STFODE 2983

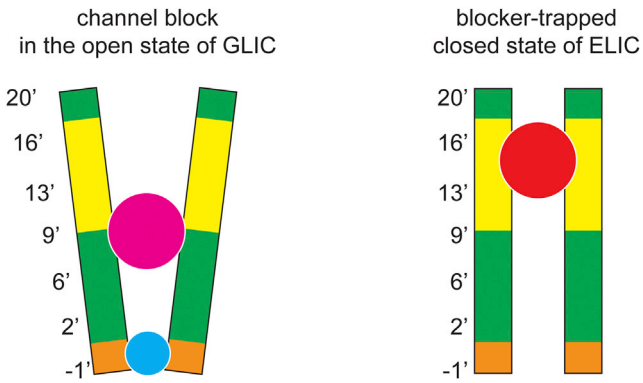

Figure 5. Model of Pore Block

Schematic illustration of the mechanism of open channel block compared to closed channel block. The pore-lining M2-helices are represented as rectangles with hydrophilic regions in green, hydrophobic in yellow, and charged in orange. In the open channel state, blockers can bind at a site for divalent cations (Hilf et al., 2010) (illustrated as a blue sphere), which is localized near the ion selectivity filter (−1' residue). Larger molecules, such as Br-lidocaine (Hilf et al., 2010) (illustrated as a magenta sphere) also bind the open channel state at a site midway the ion conduction pathway, which is localized near the 9' residue. In the blocker-trapped ELIC state, pore blockers such as memantine (illustrated as a red sphere) can bind at a site near the extracellular entryway of the channel pore, which is localized between 13' and 16' residues.

were fabricated from borosilicate glass (GC120TF-10, Harvard Apparatus) using a two stage horizontal puller (P-87, Sutter Instrument) and filled with 3 M KCl. Pipette resistances ranged from 1.0–2.0 MΩ. Because Ca^{2+} has been shown to inhibit the ELIC pore (Zimmermann et al., 2012), and this could complicate the interpretation of other pore blocking effects, oocytes were perfused with Ca^{2+}-free ND96 (96 mM NaCl, 2 mM KCl, 1 mM $MgCl_2$, 5 mM HEPES, pH 7.5) at a constant rate of 12 ml/min. Drugs were dissolved in the same saline and applied to oocytes using a simple gravity fed system calibrated to run at the same rate. Inhibition by test compounds was measured at the GABA EC_{50} for each mutant receptor.

Analysis and curve fitting was performed using Prism v4.03 (GraphPad Software, San Diego, California, USA). Concentration-response data for each oocyte were normalized to the maximum current for that oocyte. The mean and SEM for a series of oocytes were plotted against agonist or antagonist concentration and iteratively fitted to the following equation:

$$I_A = I_{min} + \frac{I_{max} - I_{min}}{1 + 10^{n_H(\log A_{50} - \log A)}},$$

where A is the concentration of ligand present; I_A is the current in the presence of ligand concentration A; I_{min} is the current when $A = 0$; I_{max} is the current when $A = \infty$, A_{50} is the concentration of A which evokes a current equal to $(I_{max} + I_{min})/2$; and n_H is the Hill coefficient.

FLEXstation Experiments

These were performed as previously described (Price and Lummis, 2005). Briefly, cells were gently rinsed twice with buffer (10 mM HEPES, 115 mM NaCl, 1 mM KCl, 1 mM $CaCl_2$, 1 mM $MgCl_2$, 10 mM glucose, pH 7.4) and 100 μl fluorescent membrane-potential sensitive dye (Molecular Devices) added. Cells were then incubated at room temperature for 45 min before assay. Fluorescence was measured in a FLEXstation (Molecular Devices) every 2 s using the acquisition software SOFTmax PRO v4.3. (Molecular Devices) GABA (0.3−300 mM) or buffer was added after 20 s. Memantine (1−300 μM) was preincubated for 5 min before assay.

Voltage Clamp Fluorometry

VCF experiments were carried out as previously described (Pless et al., 2007). In brief, an inverted Nikon Eclipse TE300 microscope (Nikon Instruments) was equipped with a high-Q TRITC filter set (Chroma Technology), and a Lambda LS 175-W xenon arc lamp was used as a light source. Excitation and emission wavelengths were selected using a Lambda 10-2 unit (Sutter Instruments). A Plan Fluor X40 objective lens (Nikon Instruments) was used to focus light on the dark pole of the oocyte, and fluorescent light was detected using a PMT400 photomultiplier tube (IonOptix) connected to the side port of the microscope. Oocytes were perfused with regular ND-96 solution (96 mM NaCl, 2 mM KCl, 1.8 mM $CaCl_2$, 1 mM $MgCl_2$, 5 mM HEPES, pH 7.5). Ca^{2+} was included in recording solution for VCF experiments as this accelerates the kinetics of ELIC (Spurny et al., 2012) and reduces possible photobleaching during the time course of our experiments. VCF recordings were done in a custom recording chamber as described (Dahan et al., 2004) using an automated Valvebank 8 perfusion system (AutoMate Scientific). Fluorescence and current signals were simultaneously acquired at a sampling frequency of 200 Hz using a Digidata 1322A interface and Clampex 9.2 software (Molecular Devices). The fluorescence signal was digitally filtered at a frequency of 1−2 Hz with an 8-pole Bessel filter for display and analysis. Electrodes for VCF recordings were filled with 3 M KCl and had a resistance near 1 MΩ. ELIC cysteine mutants for VCF experiments were constructed in the background of cysteine-free ELIC (C300S+C313S), which has functional properties that are indistinguishable from wild-type (WT) ELIC. Oocytes injected with ELIC mRNA were fluorescently labeled 3−5 days after injection by a 1 min incubation in a solution containing 10 μM methanethiosulfonate-rhodamine (MTSR, Toronto Research Chemicals) in ND96. The oocytes were then washed three times in ND96 and stored in the absence of light at 18°C until the start of recording.

Protein Expression and Crystallization

The cDNA encoding ELIC F16'S was constructed using a QuikChange (Stratagene) method and verified by sequencing (LGC Genomics). ELIC F16'S protein was expressed and purified as previously described for WT ELIC with minor modifications (Spurny et al., 2012, 2013). Briefly, ELIC F16'S was expressed as an N-terminal fusion to maltose binding protein (MBP) in the C43 *E. coli* strain. Membranes were solubilized with 2% anagrade n-undecyl-β-D-maltoside (UDM; Anatrace) and affinity purified on amylose resin (New England Biolabs), followed by cleavage with 3CV protease to remove MBP. ELIC F16'S was purified further on a Superdex 200 10/300 GL (GE Healthcare) column equilibrated with buffer containing 10 mM Na-phosphate (pH 8.0), 150 mM NaCl, and 0.15% UDM. Peak fractions corresponding to cleaved pentameric ELIC F16'S were pooled, concentrated, and supplemented with *E. coli* total lipid extract (Avanti Polar Lipids) prior to crystallization.

Crystallization of ELIC F16'S apo and complexes with memantine (Sigma-Aldrich) or bromo-memantine (synthesis described below) was carried out at 4°C by vapor diffusion of sitting drops. The crystallization buffer was composed of 200 mM ammonium sulfate, 50 mM (N-(2-acetamido)iminodiacetic acid) pH 6.5, and 9%−12% PEG4000. Crystals of ELIC F16'S in complex with memantine or bromo-memantine were obtained in the presence of 10 mM memantine and 8 mM bromo-memantine. Crystals were harvested by adding 30% glycerol as a cryoprotectant to the mother liquor and immersed in liquid nitrogen.

Structure Determination and Refinement

X-ray diffraction data sets for ELIC F16'S apo and complexes with memantine or bromo-memantine were collected at beamline X06A of the Swiss Light Source (Paul Scherrer Institute) and reached resolution limits of 3.5 Å, 3.2 Å, and 3.9 Å, respectively. For the ELIC structure in complex with bromo-memantine, we used the 3.9 Å data for structure refinement (data set 1 in Table 2). To aid the interpretation of ligand density, we calculated anomalous difference density maps using reflections to 5 Å from a higher redundancy data set obtained by merging data from different crystals (data set 1 and 2 in Table 2). Full crystallographic statistics are reported in Table 2. Data integration was done in XDS (Kabsch, 2010) and scaling in SCALA (Winn et al., 2011). Model building and refinement was carried out by iterative cycles of manual rebuilding in COOT (Emsley et al., 2010) and refinement in PHENIX (Adams et al., 2010). AutoNCS in PHENIX was used to automatically detect noncrystallographic symmetry (NCS) restraints, which were maintained during refinement for an entire subunit per NCS group. There was one Translation/Libration/Screw body that was assigned per subunit. Ligand restraints for memantine and bromo-memantine were generated using ELBOW in the

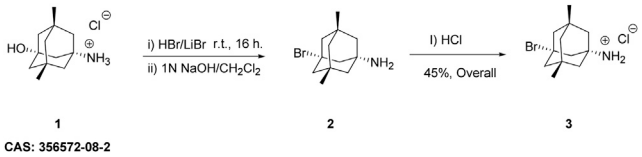

Figure 6. Synthetic Scheme for Bromo-Memantine

PHENIX suite. Model validation was done using MOLPROBITY (Chen et al., 2010), and all figures were prepared using PyMOL. The analysis of pore dimensions was carried out using HOLE (Smart et al., 1996).

Synthesis of Bromo-Memantine

The synthetic scheme for bromo-memantine is presented in Figure 6. To a solution of hydroxyadamantyl amine hydrochloride 1 (200 mg. and 0.86 mmol) in HBr (5 ml), LiBr (3 eq., 2.59 mmol, 225 mg) was added at room temperature.

The reaction mixture was stirred at room temperature for 16 hr. Upon completion of the reaction (liquid chromatography-tandem mass spectrometry [LC-MS] and thin layer chromatography monitoring), the reaction mixture was basified at 0°C with 1N NaOH and extracted with CH_2Cl_2 (4×, 50 ml). The combined organic layers were dried over $MgSO_4$, filtered, and evaporated to afford 3-bromoadamantylamine derivative 2 as a free base that was used in the next step without further purification. To crude material 2, a solution of 4N HCl in dry dioxane (3 ml) was added at room temperature. The mixture was stirred at room temperature, for 4 hr then 1 hr at 0°C. The solid that precipitated was collected by filtration, washed with ether, and dried under high vacuum to afford the targeted 3-bromo-5,7-dimethyl adamanly-1-amine hydrochloride 3 (114 mg, 44.8%) as a colorless powder. Compound 3 or 3-bromo-5,7-dimethyladamantyl-1-amine hydrochloride, is a racemic mixture termed bromo-memantine throughout this manuscript and was identified and characterized through LC-MS and ^{1}H-NMR. ^{1}H-NMR (300 MHz, DMSO-d6): δ = 0.91 (s, 6H); δ = 1.12 (d, J = 12 Hz., 1H); δ = 1.25 (d, J = 12 Hz., 1H); δ = 1.43 (d, J = 12 Hz., 2H); d = 1.52 (d, J = 12 Hz., 2H); δ = 1.89 (d, J = 12 Hz., 2H); δ = 1.95 (d, J = 12 Hz., 2H); δ = 2.22 (s, 2H); and δ = 8.09 (s, br., 3H).

ACCESSION NUMBERS

Structure factors and coordinates for ELIC F16'S apo and complexes with Br-memantine or memantine are deposited in the Protein Data Bank with accession codes 4TWH, 4TWD, and 4TWF, respectively.

SUPPLEMENTAL INFORMATION

Supplemental Information includes one figure and three 3D molecular structures and can be found with article online at http://dx.doi.org/10.1016/j.str.2014.07.013.

ACKNOWLEDGMENTS

Financial support was from the Wellcome Trust to S.C.R.L.; Onderzoekstoelage OT/13/095; FWO-Vlaanderen G.0743.10, G.0939.11, G.0762.13; and IWT-O&O-110448 to C.U.. S.C.R.L. is a Wellcome Trust Senior Research Fellow in Basic Biomedical Studies.

We thank local contacts at beamline X06A of the Swiss Light Source for assistance during data collection.

Received: May 13, 2014
Revised: July 24, 2014
Accepted: July 25, 2014
Published: September 4, 2014

REFERENCES

Adams, P.R. (1977). Voltage jump analysis of procaine action at frog end-plate. J. Physiol. *268*, 291–318.

Adams, P.D., Afonine, P.V., Bunkóczi, G., Chen, V.B., Davis, I.W., Echols, N., Headd, J.J., Hung, L.-W., Kapral, G.J., Grosse-Kunstleve, R.W., et al. (2010). PHENIX: a comprehensive Python-based system for macromolecular structure solution. Acta Crystallogr. D Biol. Crystallogr. *66*, 213–221.

Alqazzaz, M., Thompson, A.J., Price, K.L., Breitinger, H.-G., and Lummis, S.C.R. (2011). Cys-loop receptor channel blockers also block GLIC. Biophys. J. *101*, 2912–2918.

Aracava, Y., Pereira, E.F.R., Maelicke, A., and Albuquerque, E.X. (2005). Memantine blocks alpha7* nicotinic acetylcholine receptors more potently than n-methyl-D-aspartate receptors in rat hippocampal neurons. J. Pharmacol. Exp. Ther. *312*, 1195–1205.

Bocquet, N., Nury, H., Baaden, M., Le Poupon, C., Changeux, J.-P., Delarue, M., and Corringer, P.-J. (2009). X-ray structure of a pentameric ligand-gated ion channel in an apparently open conformation. Nature *457*, 111–114.

Bouzat, C. (2012). New insights into the structural bases of activation of Cys-loop receptors. J. Physiol. Paris *106*, 23–33.

Buisson, B., and Bertrand, D. (1998). Open-channel blockers at the human alpha4beta2 neuronal nicotinic acetylcholine receptor. Mol. Pharmacol. *53*, 555–563.

Chen, V.B., Arendall, W.B., 3rd, Headd, J.J., Keedy, D.A., Immormino, R.M., Kapral, G.J., Murray, L.W., Richardson, J.S., and Richardson, D.C. (2010). MolProbity: all-atom structure validation for macromolecular crystallography. Acta Crystallogr. D Biol. Crystallogr. *66*, 12–21.

Dahan, D.S., Dibas, M.I., Petersson, E.J., Auyeung, V.C., Chanda, B., Bezanilla, F., Dougherty, D.A., and Lester, H.A. (2004). A fluorophore attached to nicotinic acetylcholine receptor beta M2 detects productive binding of agonist to the alpha delta site. Proc. Natl. Acad. Sci. USA *101*, 10195–10200.

Emsley, P., Lohkamp, B., Scott, W.G., and Cowtan, K. (2010). Features and development of Coot. Acta Crystallogr. D Biol. Crystallogr. *66*, 486–501.

Gonzalez-Gutierrez, G., Lukk, T., Agarwal, V., Papke, D., Nair, S.K., and Grosman, C. (2012). Mutations that stabilize the open state of the Erwinia chrisanthemi ligand-gated ion channel fail to change the conformation of the pore domain in crystals. Proc. Natl. Acad. Sci. USA *109*, 6331–6336.

Hibbs, R.E., and Gouaux, E. (2011). Principles of activation and permeation in an anion-selective Cys-loop receptor. Nature *474*, 54–60.

Hilf, R.J.C., and Dutzler, R. (2008). X-ray structure of a prokaryotic pentameric ligand-gated ion channel. Nature *452*, 375–379.

Hilf, R.J.C., and Dutzler, R. (2009). Structure of a potentially open state of a proton-activated pentameric ligand-gated ion channel. Nature *457*, 115–118.

Hilf, R.J.C., Bertozzi, C., Zimmermann, I., Reiter, A., Trauner, D., and Dutzler, R. (2010). Structural basis of open channel block in a prokaryotic pentameric ligand-gated ion channel. Nat. Struct. Mol. Biol. *17*, 1330–1336.

Kabsch, W. (2010). XDS. Acta Crystallogr. D Biol. Crystallogr. *66*, 125–132.

Oliver, D., Ludwig, J., Reisinger, E., Zoellner, W., Ruppersberg, J.P., and Fakler, B. (2001). Memantine inhibits efferent cholinergic transmission in the cochlea by blocking nicotinic acetylcholine receptors of outer hair cells. Mol. Pharmacol. *60*, 183–189.

Pan, J., Chen, Q., Willenbring, D., Yoshida, K., Tillman, T., Kashlan, O.B., Cohen, A., Kong, X.-P., Xu, Y., and Tang, P. (2012). Structure of the pentameric ligand-gated ion channel ELIC cocrystallized with its competitive antagonist acetylcholine. Nat. Commun. *3*, 714.

Pless, S.A., Dibas, M.I., Lester, H.A., and Lynch, J.W. (2007). Conformational variability of the glycine receptor M2 domain in response to activation by different agonists. J. Biol. Chem. *282*, 36057–36067.

Prevost, M.S., Sauguet, L., Nury, H., Van Renterghem, C., Huon, C., Poitevin, F., Baaden, M., Delarue, M., and Corringer, P.-J. (2012). A locally closed conformation of a bacterial pentameric proton-gated ion channel. Nat. Struct. Mol. Biol. *19*, 642–649.

Price, K.L., and Lummis, S.C.R. (2005). FlexStation examination of 5-HT3 receptor function using Ca2+ - and membrane potential-sensitive dyes: advantages and potential problems. J. Neurosci. Methods *149*, 172–177.

Rammes, G., Rupprecht, R., Ferrari, U., Zieglgänsberger, W., and Parsons, C.G. (2001). The N-methyl-D-aspartate receptor channel blockers memantine, MRZ 2/579 and other amino-alkyl-cyclohexanes antagonise 5-HT(3) receptor

currents in cultured HEK-293 and N1E-115 cell systems in a non-competitive manner. Neurosci. Lett. *306*, 81–84.

Rogawski, M.A., and Wenk, G.L. (2003). The neuropharmacological basis for the use of memantine in the treatment of Alzheimer's disease. CNS Drug Rev. *9*, 275–308.

Sauguet, L., Shahsavar, A., Poitevin, F., Huon, C., Menny, A., Nemecz, À., Haouz, A., Changeux, J.-P., Corringer, P.-J., and Delarue, M. (2014). Crystal structures of a pentameric ligand-gated ion channel provide a mechanism for activation. Proc. Natl. Acad. Sci. USA *111*, 966–971.

Schnell, J.R., and Chou, J.J. (2008). Structure and mechanism of the M2 proton channel of influenza A virus. Nature *451*, 591–595.

Sine, S.M. (2012). End-plate acetylcholine receptor: structure, mechanism, pharmacology, and disease. Physiol. Rev. *92*, 1189–1234.

Smart, O.S., Neduvelil, J.G., Wang, X., Wallace, B.A., and Sansom, M.S. (1996). HOLE: a program for the analysis of the pore dimensions of ion channel structural models. J Mol Graph *14*, 354–360.

Spurny, R., Ramerstorfer, J., Price, K., Brams, M., Ernst, M., Nury, H., Verheij, M., Legrand, P., Bertrand, D., Bertrand, S., et al. (2012). Pentameric ligand-gated ion channel ELIC is activated by GABA and modulated by benzodiazepines. Proc. Natl. Acad. Sci. USA *109*, E3028–E3034.

Spurny, R., Billen, B., Howard, R.J., Brams, M., Debaveye, S., Price, K.L., Weston, D.A., Strelkov, S.V., Tytgat, J., Bertrand, S., et al. (2013). Multisite binding of a general anesthetic to the prokaryotic pentameric Erwinia chrysanthemi ligand-gated ion channel (ELIC). J. Biol. Chem. *288*, 8355–8364.

Stouffer, A.L., Acharya, R., Salom, D., Levine, A.S., Di Costanzo, L., Soto, C.S., Tereshko, V., Nanda, V., Stayrook, S., and DeGrado, W.F. (2008). Structural basis for the function and inhibition of an influenza virus proton channel. Nature *451*, 596–599.

Thompson, A.J., Alqazzaz, M., Ulens, C., and Lummis, S.C.R. (2012). The pharmacological profile of ELIC, a prokaryotic GABA-gated receptor. Neuropharmacology *63*, 761–767.

Wang, Q., Pless, S.A., and Lynch, J.W. (2010). Ligand- and subunit-specific conformational changes in the ligand-binding domain and the TM2-TM3 linker of alpha1 beta2 gamma2 GABAA receptors. J. Biol. Chem. *285*, 40373–40386.

Winn, M.D., Ballard, C.C., Cowtan, K.D., Dodson, E.J., Emsley, P., Evans, P.R., Keegan, R.M., Krissinel, E.B., Leslie, A.G.W., McCoy, A., et al. (2011). Overview of the CCP4 suite and current developments. Acta Crystallogr. D Biol. Crystallogr. *67*, 235–242.

Zimmermann, I., and Dutzler, R. (2011). Ligand activation of the prokaryotic pentameric ligand-gated ion channel ELIC. PLoS Biol. *9*, e1001101.

Zimmermann, I., Marabelli, A., Bertozzi, C., Sivilotti, L.G., and Dutzler, R. (2012). Inhibition of the prokaryotic pentameric ligand-gated ion channel ELIC by divalent cations. PLoS Biol. *10*, e1001429.